Observed reflectivity of the western boundary of the equatorial Pacific Ocean

Xiaoyun Zang[1] and Lee-Lueng Fu
Jet Propulsion Laboratory, California Institute of Technology, Pasadena, California, USA

Carl Wunsch
Department of Earth, Atmospheric and Planetary Sciences, Massachusetts Institute of Technology, Cambridge, Massachusetts, USA

Received 15 November 2000; revised 30 November 2001; accepted 19 December 2001; published 16 October 2002.

[1] Published claims that the reflectivity of the western boundary of the equatorial Pacific is near 100% are examined by using TOPEX/Poseidon data from October 1992 to February 2000. We perform a Fourier analysis of sea surface height measurements and define the variability consistent with the Rossby wave and Kelvin wave dispersion relationship as the energy of Rossby wave and Kelvin wave, respectively. Basin-scale Rossby waves dominate in the period ranges of 180–250 and 270–450 days. Their largest amplitudes are at 4° and 6°N, respectively. Kelvin waves dominate in distinguishable period ranges of 67–76 and 106–170 days. Because the wavelengths of the Kelvin waves generated from the reflection of low-frequency Rossby waves are much longer than the width of the basin, they cannot be readily differentiated from large-scale forced motions. An upper bound on the reflection coefficient of the Rossby wave is thus estimated as 31% for Rossby waves with periods of 180–250 days. The duration of TOPEX/Poseidon data is too short for studying the reflectivity of the lower-frequency Rossby waves. *INDEX TERMS:* 4231 Oceanography: General: Equatorial oceanography; 4275 Oceanography: General: Remote sensing and electromagnetic processes (0689); 4556 Oceanography: Physical: Sea level variations; *KEYWORDS:* western boundary reflection, equatorial Rossby waves, equatorial Kelvin waves, sea level variations, El Niño

Citation: Zang, X., L.-L. Fu, and C. Wunsch, Observed reflectivity of the western boundary of the equatorial Pacific Ocean, *J. Geophys. Res.*, *107*(C10), 3150, doi:10.1029/2000JC000719, 2002.

1. Introduction

[2] The extent to which wavelike motions in the ocean reflect from boundaries, whether lateral or vertical, has major implications for the ocean circulation. In particular, reflectivity of the western boundary in the presence of low-latitude baroclinic Rossby and Kelvin (both boundary and equatorial) waves in the Pacific Ocean is a critical element of the so-called delayed oscillator theory of the El Niño–Southern Oscillation (ENSO) [e.g., *Schopf and Suarez*, 1988; *Battisti*, 1988; *Battisti and Hirst*, 1989; *Picaut et al.*, 1997]. In this theory the oscillatory nature of ENSO depends on the efficiency of the reflection of Rossby waves into Kelvin waves at the western boundary of the tropical Pacific.

[3] *White et al.* [1990] analyzed 17 month sea level measurements from Geosat altimeter data and claimed to observe the reflection of annual period Rossby waves at the western boundary of the tropical Pacific. However, they did not obtain a quantitative estimate of the reflectivity. Subsequently, *White and Tai* [1992] used 2.7 years of Geosat data to examine the reflection of interannual Rossby waves. By assuming perfect reflection at the western boundary they determined the percent contribution that each incident Rossby wave had made to the reflected Kelvin wave. They found that the amplitude of the first meridional mode Rossby wave accounted for 70–80% of the reflected Kelvin wave amplitude with the remainder in higher meridional modes, but the records were very short. More recently, *Boulanger and Menkes* [1999] analyzed the TOPEX/Poseidon altimeter data and concluded, surprisingly, that the reflection coefficient of the western boundary was nearly 100%. The method used by *Boulanger and Menkes* [1999] to estimate the contributions of Rossby waves and Kelvin waves to observed sea surface height variability is similar to that used by *White and Tai* [1992] and will be described in section 2.

[4] The western boundary of the Pacific Ocean is an extremely complex region of islands and rough topography, and it has always been difficult to understand how the reflection of long Rossby waves could be very effective. The pioneering work on wave reflection processes in the

[1]Now at Department of Earth, Atmospheric and Planetary Sciences, Massachusetts Institute of Technology, Cambridge, Massachusetts, USA.

0148-0227/02/2000JC000719$09.00

equatorial ocean was due to *Moore* [1968] and *Moore and Philander* [1977]. *Clarke* [1983] then derived analytical expressions for the reflectivity of Rossby waves from a solid meridional wall. *Clarke* [1991] obtained an estimate of the reflection coefficient of low-frequency Rossby waves from the irregular western boundary of the tropical Pacific. The zonal wavelength of low-frequency Rossby waves is so large that he treated the land masses forming the tropical western boundary as a combination of several islands that are infinitesimally thin in the east-west direction, approximating the reflection process as multiple reflections and transmissions between several thin islands. He found the reflected Kelvin wave amplitude to be about 83% of that which would be reflected from a solid meridional wall, in agreement with a similar study on wave reflection by *Du Penhoat and Cane* [1991]. Recently, *Pedlosky* [2001] investigated the transmission of a midlatitude barotropic Rossby wave through a meridional barrier with narrow gaps and demonstrated that in order for Kelvin's circulation theorem to be satisfied, Rossby wave energy had to pass through the gaps and the energy of the transmitted wave depended on the frequency of the incident wave. The relationship between the *Pedlosky* [2001] and *Clarke* [1991] solutions is obscure, as the latter does not explicitly invoke Kelvin's circulation theorem, which is central to the former's analysis. For present purposes it suffices to infer from the theory that reflection coefficients are expected to be significantly less than 1, even when the boundary is treated as geometrically simple.

[5] In this context, the conclusions of *Boulanger and Menkes* [1999] are surprising. They interpreted their result as support for the delayed oscillator theory. This theory is not the focus here but rather is the generic problem, the extent of which the western boundary of the tropical Pacific is reflective. Moreover, both theoretical and numerical studies suggest that the reflection of Rossby waves at the western boundary plays an important role in the redistribution of mass and energy in the western tropical Pacific [*Cane and Sarachik*, 1977; *Godfrey*, 1975; *White et al.*, 1987].

2. Estimation Methods

[6] *Boulanger and Menkes* [1995, 1999] and *Boulanger and Fu* [1996] estimated the contributions of Kelvin waves and Rossby waves to sea level variability in the TOPEX/Poseidon data. They expressed the sea surface height $\eta(x, y, t)$ as

$$\eta(x, y, t) = \sum_{j=0}^{J} r_j(x, t) P_j(y), \tag{1}$$

where $P_j(y)$ represents the meridional structure of long equatorial waves ($j = 0$ are Kelvin waves, and $j \geq 1$ are Rossby waves). Here $r_j(x, t)$ is the corresponding coefficient for meridional mode $P_j(y)$ [see, e.g., *Moore and Philander*, 1977; *Gill*, 1982]. They fit $P_j(y)$ to the data, interpreted $r_0(x, t)$ as Kelvin waves and $r_j(x, t)$, where $j \geq 1$, as long Rossby waves, and used the values of $r_j(x, t)$ at the ocean boundary to study the reflection processes.

[7] There are at least two problems: (1) $r_j(x, t)$ is a combination of free and forced waves both westward and eastward propagating. (2) As will be seen in section 3, the meridional structures $P_j(y)$ are not orthogonal. The projection of sea surface height onto $P_j(y)$ obtained by *Boulanger and Menkes* [1995] depends on a weighting factor they chose in an ad hoc way.

[8] For these reasons we will not project the sea surface height data onto $P_j(y)$. Because Rossby waves and Kelvin waves are expected to have largest amplitudes at certain latitudes, it is easy to identify Rossby waves and Kelvin waves there. We will thus estimate the contributions of Rossby waves and Kelvin waves to sea surface height variability at each latitude, finding their maxima, which will then be used to estimate the reflection coefficient. The ensuing question is how to relate the maxima of sea surface height variance associated with Rossby waves and Kelvin waves to the reflection coefficient. This issue is to be addressed in section 3.

3. Theory

[9] Reflection of equatorial waves at unbroken plain walls has been studied analytically in the β plane approximation by *Moore* [1968], *Moore and Philander* [1977], and *Clarke* [1983]. These results are briefly reviewed here. The main goal of this section is to derive the reflection coefficient from the sea surface height variance of Rossby waves at one latitude and the sea surface height variance of Kelvin waves at another latitude. As will be seen in section 5, the observed Rossby waves and Kelvin waves are of sufficiently long wavelength to be modeled in the long-wave limit.

3.1. Dispersion Relation

[10] For vertical mode n and meridional mode m the dispersion relationship is

$$\frac{\omega^2}{c_n^2} - k^2 - \frac{\beta k}{\omega} = (2m + 1)\frac{\beta}{c_n}, \tag{2}$$

where ω is radian frequency, k is the zonal wave number, and c_n is the phase speed of the nth vertical mode gravity wave obtained from the vertical eigenvalue problem. In the equatorial Pacific, $c_1 \approx 2.7$ (m s^{-1}) and $c_2 \approx 1.4$ (m s^{-1}) [e.g., *Chelton et al.*, 1998].

[11] For $m = 0$ the wave solution is the "mixed Rossby-gravity wave." For $m \geq 1$ the waves can be divided into two classes according to their frequencies: inertia gravity waves and Rossby waves. For each vertical mode, there is a maximum period for inertia gravity waves:

$$T^n_{G-\max} = \frac{2\pi}{\sqrt{\beta c_n}(1 + \sqrt{2}/2)}, \tag{3}$$

and a minimum period for Rossby waves,

$$T^n_{R-\min} = \frac{2\pi}{\sqrt{\beta c_n}(1 - \sqrt{2}/2)}. \tag{4}$$

[12] $T^1_{G-\max}$ and $T^1_{R-\min}$ are about 6 and 33 days, respectively. The inertia gravity waves are not adequately sampled by TOPEX/Poseidon with its 10 day repeat cycle. The

aliased period of the 4 day peak in the TOPEX/Poseidon data is 20 days, but the amplitude is sufficiently small (1 cm) [*Wunsch and Gill*, 1976] that it is simply ignored here. For long Rossby waves the dispersion relationship is approximately

$$\omega = -\frac{kc_n}{(2m+1)}, \tag{5}$$

and for equatorial Kelvin waves it is,

$$\omega = kc_n. \tag{6}$$

3.2. Reflection Coefficient for Incoming Long Rossby Waves

[13] The solution for p and u for long Rossby waves can be written [*Gill*, 1982]

$$p(x,y,t,m) = \text{real}\left\{A_R(\omega,m)\left[\frac{\psi_{m+1}(y)}{\sqrt{2(m+1)}} + \frac{\psi_{m-1}(y)}{\sqrt{2m}}\right]e^{i(k_m x-\omega t)}\right\}, \tag{7}$$

$$u(x,y,t,m) = \text{real}\left\{\frac{A_R(\omega,m)}{c_n}\left[\frac{\psi_{m+1}(y)}{\sqrt{2(m+1)}} - \frac{\psi_{m-1}(y)}{\sqrt{2m}}\right]e^{i(k_m x-\omega t)}\right\}, \tag{8}$$

where $k_m = -[(2m+1)\,\omega]/c_n$; $A_R(\omega, M)$ is the amplitude of pressure associated with Rossby waves, and the meridional structure $\psi_m(y)$ is the normalized Hermite function of order m,

$$\psi_m(y) = \left(2^m m!\sqrt{\pi}\right)^{-\frac{1}{2}}\left(\frac{\beta}{c_n}\right)^{\frac{1}{4}}\exp\left(-\frac{\beta y^2}{2c_n}\right)H_m\left(\sqrt{\frac{\beta}{c_n}}y\right), \tag{9}$$

which satisfies the orthonormality condition

$$\int_{-\infty}^{+\infty}\psi_i(y)\psi_j(y)dy = \delta_{ij}. \tag{10}$$

[14] The meridional structure of pressure (sea surface height) associated with the mth meridional mode long Rossby wave is

$$P_m(y) = \frac{\psi_{m+1}(y)}{\sqrt{2(m+1)}} + \frac{\psi_{m-1}(y)}{\sqrt{2m}}. \tag{11}$$

These functions do not form an orthogonal set (although the underlying Hermite functions do).

[15] For the Kelvin wave,

$$p(x,y,t) = \text{real}\left[A_K(\omega)\psi_0(y)e^{iw(\frac{x}{cn}-t)}\right], \tag{12}$$

$$u(x,y,t) = \text{real}\left[\frac{A_K(\omega)}{c}\psi_0(y)e^{iw(\frac{x}{cn}-t)}\right], \tag{13}$$

where $A_K(\omega)$ represents the pressure amplitude. We will permit the various amplitudes A to be slowly varying functions of longitude, x, e.g., $A_K(x, \omega)$.

[16] The energy equation for the equatorial waves of each vertical mode can be written [*Moore and Philander*, 1977]

$$\frac{\partial}{\partial t}\left[\frac{1}{2}\left(u^2+v^2+p^2/c_n^2\right)\right] + \frac{\partial(up)}{\partial x} + \frac{\partial(vp)}{\partial y} = 0. \tag{14}$$

The zonal energy flux across any longitude $x = x_0$ is

$$F(x_0) = \int_{-\infty}^{+\infty}(\overline{up})dy, \tag{15}$$

where the overbar denotes the time average. Substitution of equations (12) and (13) into (15) gives the energy flux of Kelvin wave across longitude x_0:

$$F_K(x_0,\omega) = \frac{|A_K(x_0,\omega)|^2}{2c_n}. \tag{16}$$

The corresponding energy flux of the mth meridional mode Rossby wave is

$$F_R(x_0,\omega,m) = -\frac{|A_R(x_0,\omega,m)|^2}{4c_n m(m+1)}, \tag{17}$$

where the minus sign indicates that the energy flux is westward.

[17] The reflection of the Mth meridional mode Rossby wave from a solid meridional western boundary consists of a finite number of short-wavelength Rossby waves ($m \le M$) whose group velocity is eastward and an equatorial Kelvin wave (when M is odd) or a short-wavelength mixed Rossby-gravity wave (when M is even) [e.g., *Clarke*, 1983] with both of the latter having eastward group velocities. Short-wavelength Rossby waves and mixed Rossby-gravity waves tend to be dissipated near the western boundary. Therefore one expects to see primarily Kelvin waves carrying energy eastward far from the boundary.

[18] An expression for the reflection coefficient of general Rossby waves was derived by *Clarke* [1983]. We define the modified reflection coefficient R' at the western boundary $x = x_w$ for the incoming Mth meridional mode long Rossby wave in terms of the fraction of the power appearing in the reflected Kelvin wave as

$$R'(x_w,\omega,M) = \frac{|F_K(x_w,\omega)|}{|F_R(x_w,\omega,M)|}. \tag{18}$$

[19] Substitution of equations (16) and (17) into (18) gives

$$R'(x_w,\omega,M) = 2M(M+1)\frac{|A_K(x_w,\omega)|^2}{|A_R(x_w,\omega,M)|^2}. \tag{19}$$

Figure 1 shows *Clarke*'s [1983] result for all Rossby waves. R' decreases monotonically as the meridional mode number increases and becomes very small when $M = 3$. For each meridional mode, R' decreases as frequency increases, and the long wavelength value is obtained as $\omega \to 0$, which is 1/2 for $M = 1$, 1/8 for $M = 3$, and 1/16 for $M = 5$. Note that R' is zero for even M because then the reflection consists of a finite number of short-wavelength Rossby waves and a

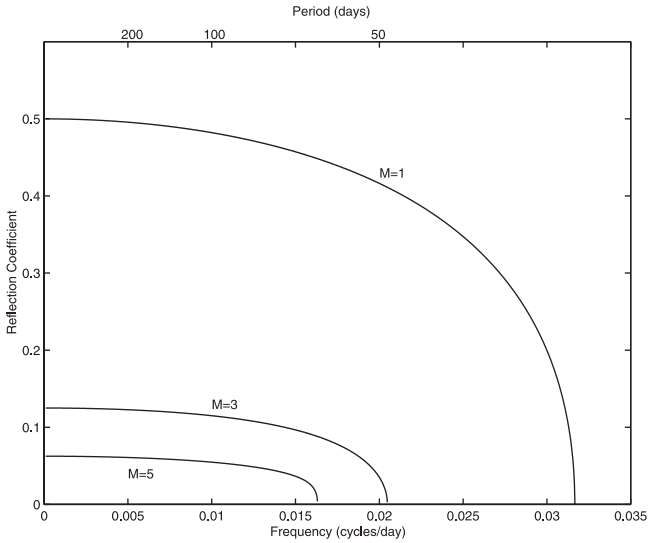

Figure 1. The reflection coefficient for incoming Rossby waves with meridional mode number $M = 1$, 3, and 5 from a solid meridional western boundary with a flat bottom [*Clarke*, 1983].

short-wavelength mixed Rossby-gravity wave and no Kelvin wave.

[20] Equation (19) relates the reflection coefficient to the wave amplitudes $A_R(x_w, \omega, M)$ and $A_K(x_w, \omega)$. As discussed in section 2, $A_R(x_w, \omega, M)$ and $A_K(x_w, \omega)$ cannot be readily obtained from the sea surface height data. We will instead estimate the sea surface height variance associated with Rossby waves and Kelvin waves latitude by latitude.

[21] Define the sea surface height variance of the mth mode long Rossby wave at $y = y_1$, $x = x_w$, as $E_R(y_1, x_w, \omega, m)$, and the sea surface height variance of the Kelvin wave at $y = y_2$, $x = x_w$, as $E_K(y_2, x_w, \omega)$, then

$$E_R(y_1, x_w, \omega, m) = \frac{1}{2}|A_R(x_w, \omega, m)|^2 |P_m(y_1)|^2 \qquad (20)$$

$$E_K(y_2, x_w, \omega) = \frac{1}{2}|A_K(x_w, \omega)|^2 |\psi_0(y_2)|^2. \qquad (21)$$

Substitution of equations (20) and (21) into (19) yields the modified reflection coefficient of a Mth meridional mode long Rossby wave:

$$R'(x_w, \omega, M) = 2M(M+1)\frac{|P_M(y_1)|^2}{|\psi_0(y_2)|^2}\frac{E_K(x_w, y_2, \omega)}{E_R(x_w, y_1, \omega, M)}. \qquad (22)$$

Equation (22) is the primary focus of this study: it relates the reflection coefficient to the sea surface height variance of a Rossby wave at one latitude and to the sea surface height variance of the Kelvin wave at another latitude. Note that y_1 and y_2 in equation (22) are indefinite. As will be seen in section 5.3, y_1 and y_2 are chosen to be the latitudes where Rossby waves and Kelvin waves have largest amplitudes, respectively.

4. Data and Data Processing

[22] The first 274 cycles, October 1992 to February 2000, of the along-track altimetric data from TOPEX/Poseidon [*Fu et al.*, 1994] were used here. The data were mapped onto a regular grid with a spacing of 2° longitude and 0.5° latitude at 9.91 day time intervals using a Gaussian mapping technique. TOPEX/Poseidon measurements are irregular in space, and there is a time lag between measurements at different places within one orbit cycle. For slowly propagating baroclinic waves in middle latitude the neglect of this asynoptic sampling feature is justifiable, but is less so for equatorially trapped waves. To minimize the error, the mapping was carried out in two steps. First, the data were interpolated onto a common time grid with a spacing of 9.91 days at each along-track sampling point. The data were then mapped spatially onto a regular grid of 2° longitude and 0.5° latitude. Because the equatorially trapped waves are characterized by very short meridional scales, the meridional decorrelation scale for mapping is set to 0.13°, and the zonal decorrelation scale is 4°. Note that although the zonal spacing between tracks is about 3°, the meridional resolution of along-track data is very high, about 0.05°. The temporal mean of the data at each spatial point was removed. In this study we focus on analyzing the sea surface height anomalies at those latitudes displayed in Figure 2.

5. Results

5.1. Kelvin Waves

[23] The frequency spectra of sea surface height anomalies at each gridded point along the equator were estimated. Figure 3 shows how the power of sea surface height depends on frequency and longitude at the equator; it is dominated by the low frequencies with an energy trough near the 700 day period. Near 550 day periods, variability in the region near the dateline is relatively weak. Significant variance is found around periods of 6 months and 1 year. At a period of 1 year, strong variability is observed over the central Pacific. Near 6 month periods the variability east of 200°E is stronger. Strong variability is also found east of 240°E around 210 days.

[24] Figure 4 shows that the zonal wave number spectrum along the equator is red and roughly proportional to k^{-2}. In contrast, the globally averaged wave number spectrum follows $k^{-2.5}$ and $k^{-1/2}$ relations at wavelengths shorter and longer than about 400 km, respectively [e.g., *Wunsch*

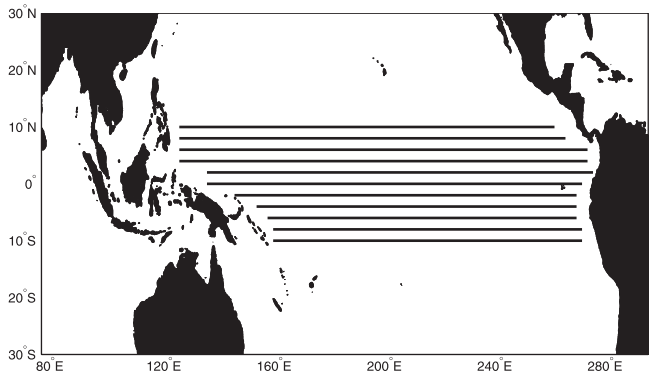

Figure 2. Zonal dark lines, which range from 10°S to 10°N with an increment of 2°, are those latitudes along which zonal wave number/frequency spectra of sea surface height anomalies are to be analyzed.

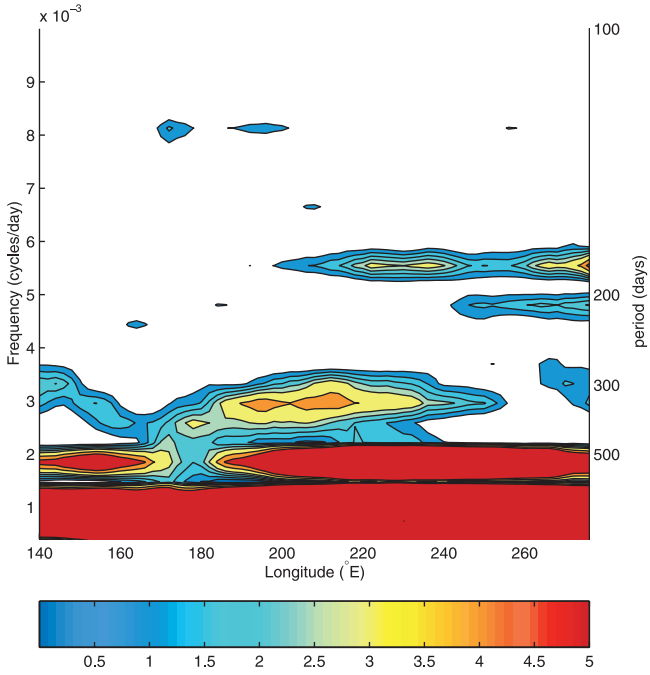

Figure 3. The power of sea surface height (cm^2) at the equator as a function of frequency and longitude.

and Stammer, 1995]. Unlike the mid-atitude ocean, which is dominated by mesoscale eddies with wavelengths of about 400 km, the equator is dominated by basin-scale motions.

[25] The zonal wave number/frequency spectrum of sea surface height anomalies was computed using a two-dimensional fast Fourier transform method to differentiate eastward propagating from westward propagating energy. To obtain statistically stable estimates, a nonoverlapping average over five adjacent frequency bands was formed. The two-dimensional spectrum shown in Figure 5 thus has about 10 degrees of freedom for each estimate. The corresponding frequency band width is 0.0018 cycles per day, and the centers of the frequency bands are near 900, 338, 208, 150, . . . , 20 days.

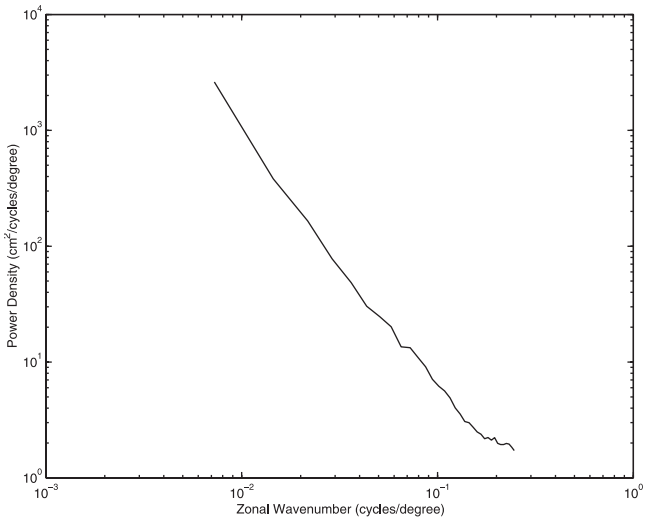

Figure 4. Temporally averaged zonal wave number spectrum of sea surface height anomalies at the equator.

The first three frequency bands are dominated by the ENSO, annual, and semiannual cycles, respectively.

[26] As expected, there is more energy going eastward than westward at the equator (Figure 5). Energy maxima at periods longer than 175 days are indistinguishable from a wave number $k = 0$. About 60% of the variability in the period range of 180–250 days is also near $k = 0$. Note that the energy at $k = 0$ consists not only of nonpropagating motions but also of propagating waves with wavelengths longer than the width of the basin. The period of the first baroclinic Kelvin wave with wavelength equal to the width of the equatorial Pacific (about 140°) is 70 days. At longer periods the wavelength of the first baroclinic Kelvin wave exceeds the width of the equatorial Pacific and the apparent $k = 0$.

[27] Figure 5 shows that basin-scale eastward propagating waves dominate in the period range of 50–175 days. The most significant energy maximum is observed in the period range of 67–76 day and falls right under the dispersion curve of the first baroclinic Kelvin wave. Here "most significant" means that the percentage of energy (about 73%) lying at the maximum relative to the total energy in the period range of 67–76 days is highest. The two maxima at periods between 110 and 175 days are located very close to the dispersion curve of the second baroclinic Kelvin wave with each having 52% of the total variability at the period ranges of 110–130 and 140–175 days, respectively.

5.2. Rossby Waves

[28] Equatorial Kelvin waves have maximum amplitude at the equator, while the largest amplitude of Rossby waves

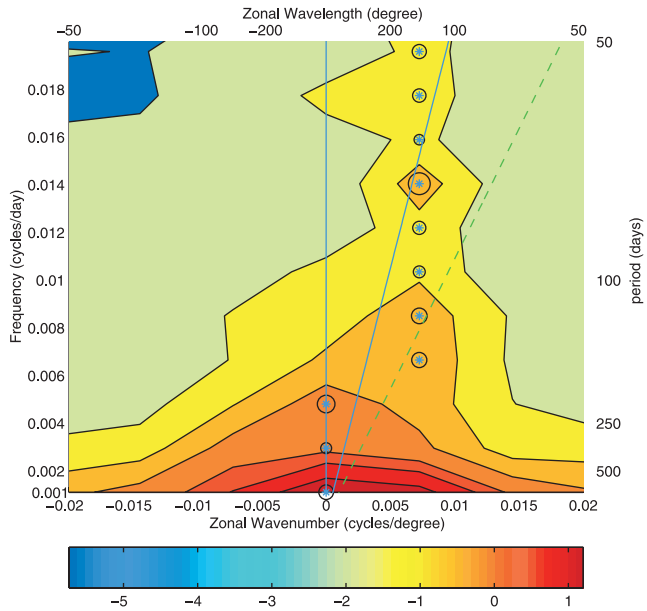

Figure 5. Zonal wave number/frequency spectrum of sea surface height anomalies (cm^2) at the equator, plotted as $\log[\Phi(\omega, k)]$ at 4°, 6°, 8°, and 10°N. The observed spectral peak in each frequency band is marked by a star. The size of the circle around the peak represents the fraction of energy lying in the observed peak relative to the total energy in each frequency band. The solid and dashed lines denote the dispersion curve of the first and second baroclinic Kelvin wave, respectively.

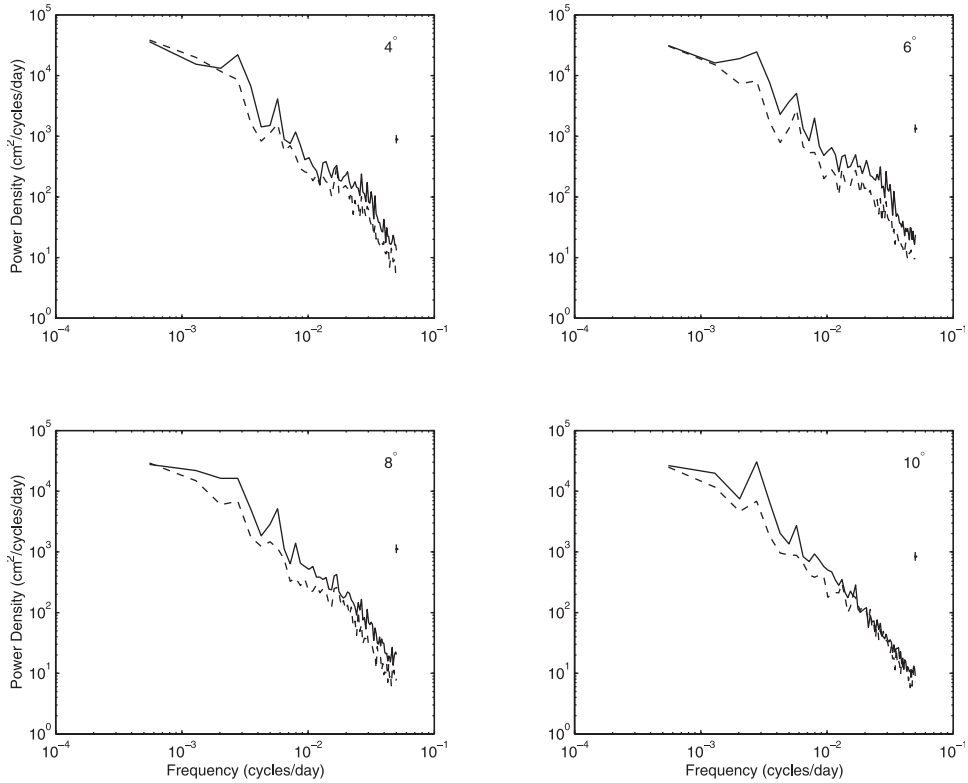

Figure 6. Zonally averaged frequency spectra of sea surface height anomalies off the equator. The spectra in the Northern Hemisphere and in the Southern Hemisphere are plotted in solid and dashed lines, respectively. Note the short 95% confidence interval.

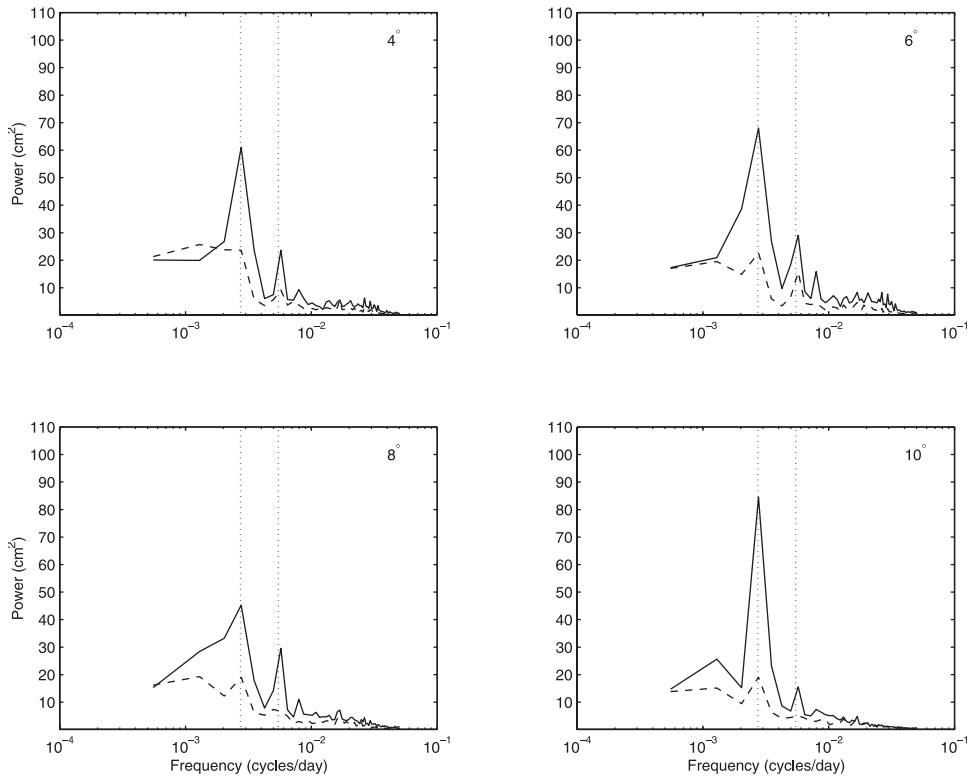

Figure 7. Corresponding variance-preserving forms of the frequency spectra shown in Figure 6. Annual and semiannual periods are denoted by dotted lines.

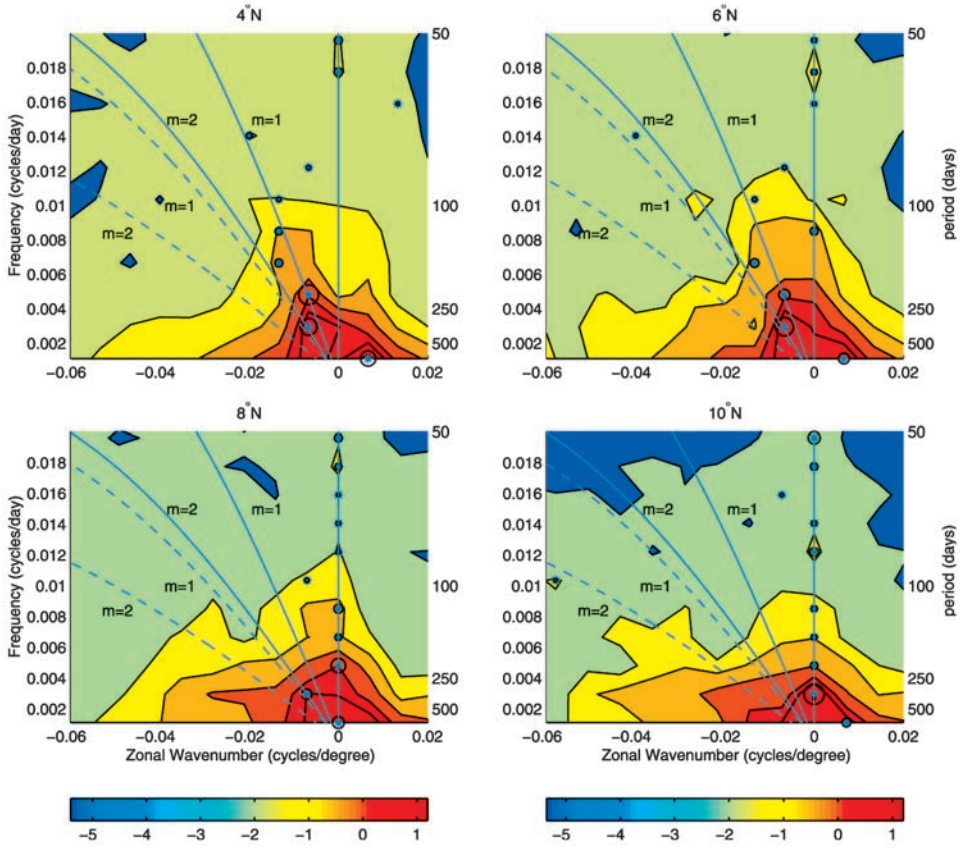

Figure 8. Zonal wave number/frequency spectrum of sea surface height anomalies (cm^2), plotted as $\log[\Phi(\omega, k)]$ at 4°, 6°, 8°, and 10°N. Superimposed are the dispersion curves for first and second meridional mode Rossby waves of the first baroclinic mode (solid curves) and the second baroclinic mode (dashed curves).

lies off the equator at a position determined by m. Figures 6 and 7 show the zonally averaged frequency spectra and the corresponding variance-preserving forms of the sea surface height anomalies off the equator. As shown, the off-equator variability is dominated by motions with periods longer than 100 days (Figure 7). There are two maxima at the annual and semiannual periods, and they are marginally significant in the Northern Hemisphere (Figure 6). Energy distribution is asymmetric: variability in the Northern Hemisphere is stronger, with the annual cycle at 6°N having about 3 times the energy at 6°S (Figure 7). Equatorial motions are dominated by interannual variability, while the off-equator regions are dominated by the annual cycle.

[29] The two-dimensional zonal wave number/frequency spectra off the equator are displayed in Figures 8 and 9 and show the dominance of westward propagating motions. At 4°N the lowest-frequency band is dominated by a basin-scale eastward propagating wave. Two significant energy maxima are observed in the period ranges of 180–250 and 270–450 days, and both are located at a wavelength of about 150° longitude. The maximum in the period range of 180–250 days is located on the dispersion curve of the first baroclinic Rossby wave with $m = 1$. The maximum in the period range of 270–450 days is very close to the dispersion curve of both the $n = 1$ Rossby wave with $m = 2$ and the $n = 2$ Rossby wave with $m = 1$. From sea surface height alone one cannot differentiate the contributions of the first and second baroclinic modes. The phase speeds of the first baroclinic Rossby wave with $m = 2$ and the second baroclinic Rossby wave with $m = 1$ are 0.54 and 0.47 (m s^{-1}), which are indistinguishable in Figure 7 because of the finite frequency and wave number bandwidth. *Lukas and Firing* [1985] and *Kessler and McCreary* [1993] found that the annual variations in hydrographic observations were consistent with Rossby waves with $m = 1$. The combination of our study of sea surface height and the independent analysis of hydrographic profiles suggests that the period range of 270–450 days is dominated by the annual Rossby wave with $m = 1$, $n = 2$.

[30] As shown in Figures 8 and 9, Rossby waves in the period ranges of 180–250 and 270–450 days are asymmetric: they tend to have larger amplitudes in the Northern Hemisphere. The observed Rossby wave in the period range of 180–250 days has largest amplitude at 4°N and is consistent with the theory for Rossby waves with $m = n = 1$. The Rossby wave, which is expected to have an amplitude maximum at 2.7° latitude, is largest at 6°N instead. The discrepancy between observations and standard theory is presumably due to wind forcing. *Kessler* [1990] found that the amplitude pattern of the annual cycle of wind stress curl in

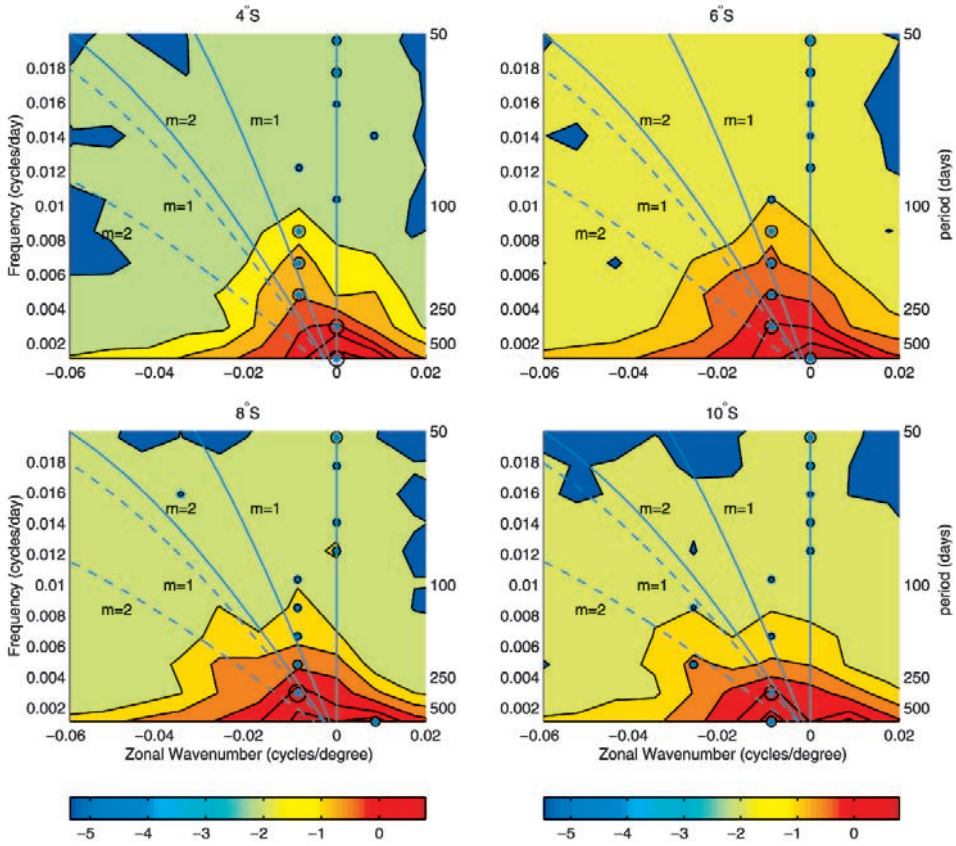

Figure 9. Same as Figure 8 except for the Southern Hemisphere.

the equatorial region was similar to that of sea surface height with a maximum near 5°–6°N.

5.3. Reflection Coefficients

[31] As shown in the preceding sections, Rossby waves dominate in the period ranges of 180–250 and 270–450 days. At periods shorter than 170 days, Rossby waves account for <20% of the variability in each frequency band. Kelvin waves dominate in the period ranges of 67–76 and 106–175 days. In the following we will estimate the reflection coefficients of the Rossby waves.

5.3.1. Reflection of Rossby Waves in the Period Range of 180–250 Days

[32] Observed Rossby waves in the period ranges of 180–250 days have largest amplitude at 4°N and account for about 63% of the total energy there. Kelvin waves generated from the reflection of these Rossby waves are expected to have a wavelength of about 440° longitude, approximately 3 times the width of the equatorial Pacific.

[33] One might attempt to estimate the energy of the reflected Kelvin wave at the western boundary by performing directional filtering of sea surface height data along the equator to retain the large-scale eastward propagating motions. In Appendix A we describe an experiment with synthetic data to compare the results from directional filtering and frequency filtering only. In the latter method we extracted the variability within a certain period range at the western boundary using a Fourier transform. The result from frequency filtering alone was found to be better. Directional filtering involves wave number filtering as well as frequency filtering. However, wave number filtering is achieved at the expense of spatial resolution. After leaving the western boundary the Kelvin wave generated from boundary reflection is modified by atmospheric forcing, mean stratification, etc. Therefore, if wave number filtering is applied, the data at the western boundary will contain some unwanted information from the interior. In addition, wave number filtering tends to distort the data near the boundary because of edge effects.

[34] Using a Fourier transform, we filtered the sea surface height anomalies at the equator and 4°N to extract the variability in the period range of 180–250 days. The time-longitude diagram of the filtered data is displayed in Figure 10. As shown there, at the equator the variability in the period range of 180–250 days near the western boundary is characterized by fast eastward propagating motions. Above all, Figure 10 shows clear evidence of western boundary reflection. Along the equator, there is a break in the eastward propagating signals at 170°–180°E: Kelvin waves generated from western boundary reflection either vanish or become amplified there. One interesting feature to note in Figure 10 is that the amplitudes of Kelvin waves tend to increase as they propagate to the east. This phenomenon has also been observed by *Susanto et al.*, [1998]. Because of the eastward shoaling of the thermocline depth, as the Kelvin wave propagates eastward, the wave amplitude has to increase in order to conserve energy [*Hughes*, 1981]. Using the WKBJ method, *Hughes* [1981] derived a simple analytic relationship between the amplitude of a

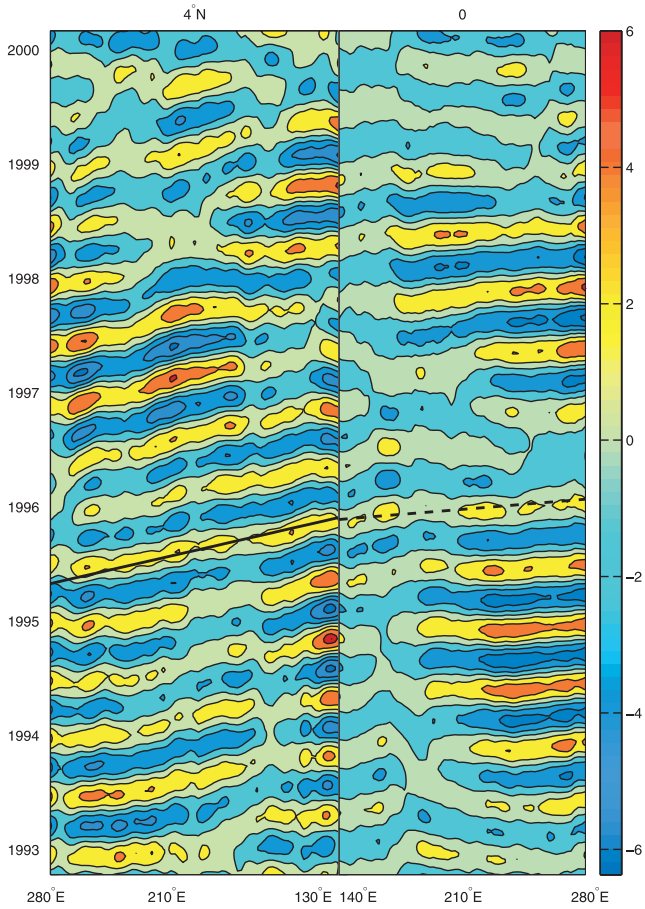

Figure 10. The time-longitude diagram of sea surface height variability (centimeters) in the period range of 180–250 days (left) at 4°N and (right) at the equator. The slanted heavy solid line represents the phase of the long Rossby wave with $m = n = 1$, and the slanted heavy dashed line is the phase of the Kelvin wave with $n = 1$. Note that the direction of the x axis of the time-longitude diagram along 4°N has been reversed.

Kelvin wave and the thermocline depth based on energy conservation: the amplitude of the Kelvin wave increases as the thermocline depth decreases to the power −3/8.

[35] Figure 11 shows that the sea surface height variability in the period range of 180–250 days at the western boundary at the equator is weaker than that at the western boundary at 4°N. However, the sea surface heights variability at the equator and 4°N have the same phase most of the time, and their correlation coefficient is 0.77. The variance of sea surface height in the period range of 180–250 days at the western boundary (x = 130°E) at 4°N is 8.8 cm^2. Because about 63% of sea surface height variability along 4°N is consistent with Rossby wave dispersion relation, the sea surface height variance associated with Rossby wave at the western boundary (x = 130°E) at 4°N is

$$E_R(x_w, y = 4^\circ\mathrm{N}, 1/250 < \omega < 1/180) = 8.8 \times 0.63 = 5.5 \text{ cm}^2. \tag{23}$$

The variance of sea surface height in the period range of 180–250 days is 1.6 cm^2 at the western boundary (x = 140°E) at the equator. About 60% of sea surface height variability along the equator is found indistinguishable from $k = 0$, and the variability at $k = 0$ consists not only of Kelvin waves but also of large-scale forced motions; therefore 60% is a conservative upper bound of the contributions of Kelvin waves to sea surface height changes at the equator. The sea surface height variance associated with a Kelvin wave at the western boundary of the equator is

$$E_K(x_w, y = 0^\circ, 1/250 < \omega < 1/180) \le 1.6 \times 0.6 = 0.96 \text{ cm}^2. \tag{24}$$

Substitution of equations (23) and (24) into (22) yields

$$R'(x_w, 1/250 < \omega < 1/180) \le 31 \tag{25}$$

that is, 31% is a conservative upper bound on the reflection of Rossby waves in the period range of 180–250 days.

5.3.2. Reflection of Rossby Waves in the Period Range of 270–450 Days

[36] Rossby waves also dominate in the period range of 270–450 days and have largest amplitude at 6°N. Before equation (22) is used to estimate the reflection coefficient we need to ascertain if there are indeed Kelvin waves generated from the reflection of the Rossby waves. Figure 12 shows the time-longitude diagram of sea surface height variability in the period range of 270–450 days at the equator and at 6°N. As shown, at 6°N the variability in the period range of 270–450 days is dominated by westward propagating waves, and the observed phase speed is faster than that predicted from the standard theory for the second baroclinic Rossby wave with $m = 1$. No clear evidence of boundary reflection is observed in Figure 12. For example, at the beginning of 1996 a downwelling Rossby wave (positive sea surface height anomaly) arrives at the western boundary. The Kelvin wave expected from western boundary reflection is indicated by the heavy dashed line, but the observations

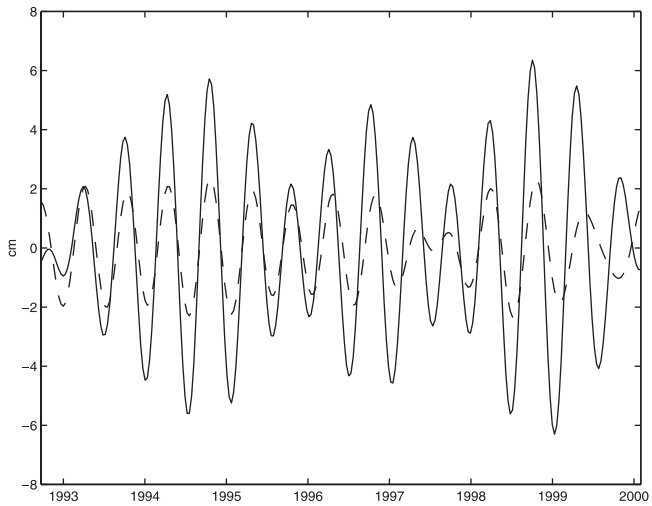

Figure 11. Time series of sea surface height variability within the band of 180–250 days at x = 130°E, y = 4°N (solid line) and at x = 140°E, y = 0 (dashed line).

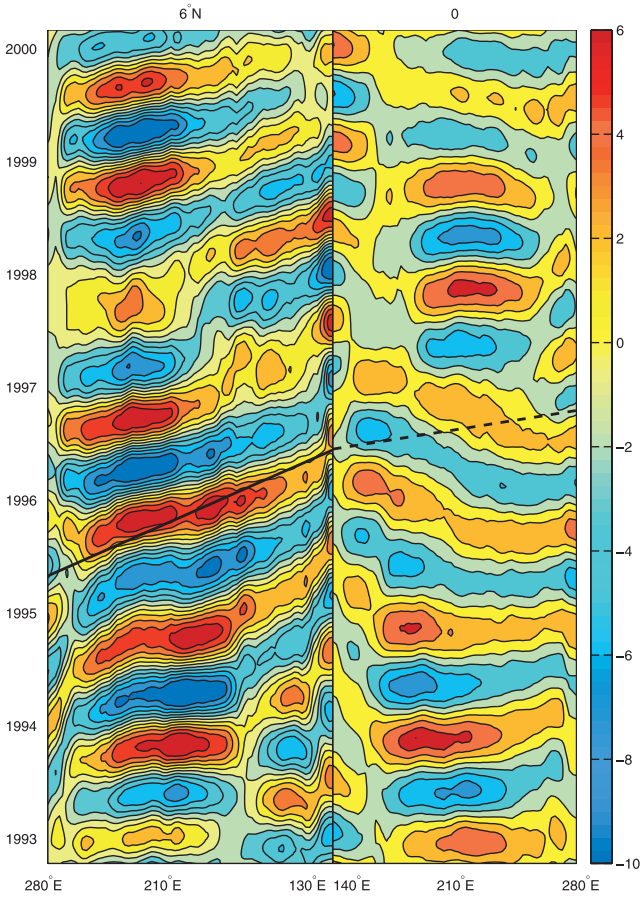

Figure 12. The time-longitude diagram of sea surface height variability (centimeters) in the period range of 270–450 days (left) at 6°N and (right) at the equator. The slanted heavy solid line represents the phase line of theoretical long Rossby wave with $m = 1$, $n = 2$, and the slanted heavy dashed line stands for the phase line of theoretical Kelvin wave with $n = 2$. The direction of the x axis of the time-longitude diagram along 6°N has been reversed.

are inconsistent with the expected reflection. The variability in the period range of 270–450 days near the western boundary at the equator is dominated not by Kelvin waves but by westward propagating signals. No clear evidence of Kelvin waves created from the reflection of Rossby waves can be identified at this period.

6. Conclusion and Discussion

[37] The problem of western boundary reflection is revisited here by estimating the contributions of Rossby waves and Kelvin waves to observed sea surface height variability through Fourier analysis. It is found that Rossby waves dominate in the period ranges of 180–250 and 270–450 days. Kelvin waves generated from the reflection of these Rossby waves have such long wavelengths that they cannot be easily separated from large-scale forced motions. For this reason, only an upper bound on the reflection coefficient is found: about 30% of the energy of Rossby waves in the period range of 180–250 days is reflected as Kelvin waves. No evidence of reflection of Rossby waves with periods of 270–450 days is discernible.

[38] The high reflection coefficient obtained by *Boulanger and Menkes* [1999] is partly due to the presence of both freely propagating waves and forced motions in their analysis. Because the overall variability of sea surface height is dominated by forced motions and because forced motions have very large spatial scales, it is not surprising that the data are highly correlated at the western boundary of different latitudes within the tropics, a key finding underlying their estimates of high reflectivity.

[39] The study by *Battisti* [1988] suggests that the dominant period of the waves involved in the delayed oscillator is the same as the ENSO period: 3–7 years. *Battisti and Hirst* [1989] investigated the effect of the reflectivity of the western boundary on the interannual variability in the tropics by using a simple reduced gravity model with a rectangular basin. They concluded that the amplitude of the Kelvin wave generated from western boundary reflection had to be >55% of that in the pure reflection case in order for the delayed oscillator to work. At ENSO periods the wavelength of the first baroclinic equatorial Rossby wave is more than 5 times the width of the ocean basin, and the Kelvin wave has an even longer wavelength. This prevents us from quantitatively estimating the contributions of Kelvin waves and Rossby waves to the observed sea surface height variability at the ENSO timescale.

[40] We find two significant bands of Kelvin waves: in the period ranges of 67–76 and 106–170 days. However, the Rossby wave signal is so weak in these period ranges that no estimates of reflection coefficient are possible. These Kelvin waves are unlikely to have been generated by western boundary reflection.

Appendix A

[41] We conduct an experiment here with simulated wave fields to find a good method to estimate the energy of a long

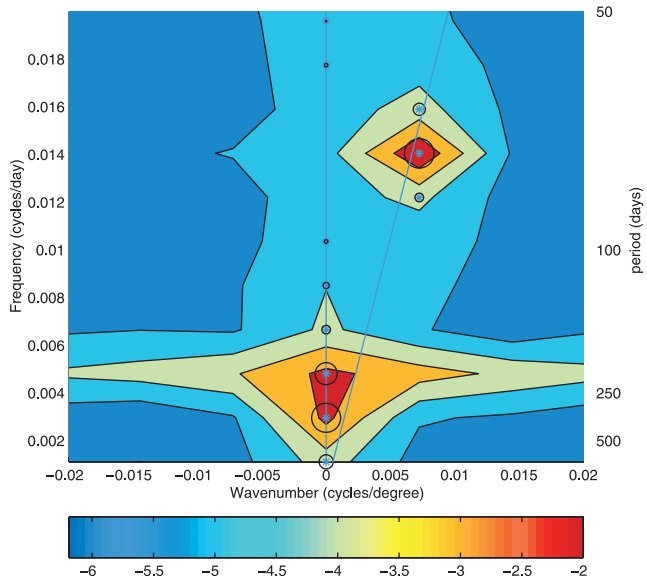

Figure A1. Same as Figure 5 except for simulated data.

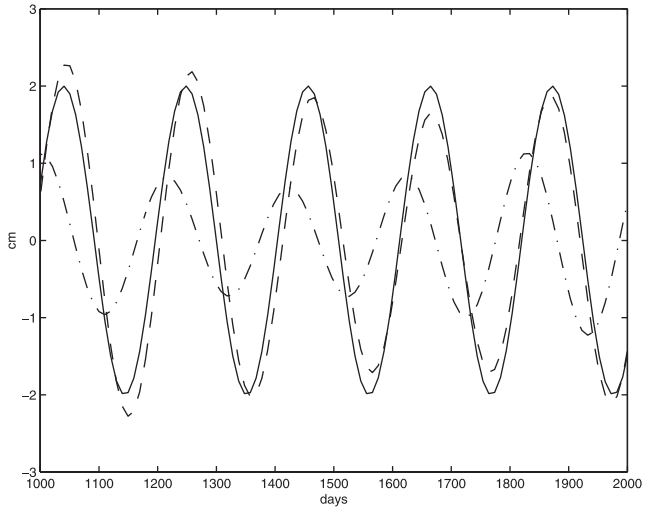

Figure A2. Time series of frequency filtered data (dashed line), two-dimensional filtered data (dash-dotted line), and true signal (solid line).

wave at the boundary. The simulated data, which consist of a zonally uniform seasonal cycle, two Kelvin waves, and white noise, are generated to mimic the observations along the equator and can be written

$$h(x,t) = a_1 \sin\left(\frac{2\pi}{L_1}x - \frac{2\pi}{T_1}t\right) + a_2 \sin\left(\frac{2\pi}{L_2}x - \frac{2\pi}{T_2}t\right) + a_3 \sin\left(\frac{2\pi}{L_3}x - \frac{2\pi}{T_3}t\right) + n(x,t), \quad \text{(A1)}$$

where $a_1 = 4.0$ cm, $a_2 = a_3 = 2.0$ cm, $L_1 = 140°$, $L_2 = 440°$, $L_3 = +\infty$, $T_1 = 71$ days, $T_2 = 208$ days, $T_3 = 360$ days, $n(x, t)$ represents the white noise, and its variance is 1.0 cm^2.

[42] The sampling spacing, zonal, and temporal length of the simulated data are identical to those of the observations along the equator. The simulated data were analyzed the same way as the observations were analyzed in section 5. Note that one simulated Kelvin wave has a wavelength equal to the width of the equatorial Pacific, and the other one has a wavelength 3 times the width of the equatorial Pacific.

[43] The frequency/wave number spectrum of simulated data is shown in Figure A1. As expected, the energy in the period range of 67–76 days is dominated by eastward going motions with a wavelength equal to the width of the basin, while the energy maximum in the period range of 180–250 days is located at $k = 0$ because the wavelength of the Kelvin wave at a period of 208 days is much longer than the width of the basin. In the following we try two different ways to estimate the energy of the Kelvin wave in the period range of 180–250 days at the western boundary. In the first method we simply perform a one-dimensional frequency filter to extract the variability in the period range of 180–250 days at the western boundary. In the second method we perform a two-dimensional filtering to retain the eastward propagating motions ($k > 0$) plus the motions at $k = 0$ in the period range of 180–250 days. The results from these two methods along with the true signal are shown in Figure A2. As shown, the result from only the frequency filtering is better than that from the two-dimensional filtering. The reasons have been discussed in section 5.3.

[44] **Acknowledgments.** The research described in the paper was partly carried out at the Jet Propulsion Laboratory, California Institute of Technology, and at Massachusetts Institute of Technology under contract with the National Aeronautics and Space Administration. Support from the TOPEX/Poseidon and Jason 1 projects is acknowledged. Comments from two anonymous reviewers and the editor helped to improve our presentation.

References

Battisti, D. S., The dynamics and thermodynamics of a warming event in a coupled tropical atmosphere/ocean model, *J. Atmos. Sci.*, *45*, 2889–2919, 1988.

Battisti, D. S., and A. C. Hirst, Interannual variability in a tropical atmosphere ocean model: Influence of the basic state, ocean geometry and nonlinearity, *J. Atmos. Sci.*, *46*, 1687–1712, 1989.

Boulanger, J.-P., and L.-L. Fu, Evidence of boundary reflection of Kelvin and first-mode Rossby waves from TOPEX/Poseidon sea level data, *J. Geophys. Res.*, *101*, 16,361–16,371, 1996.

Boulanger, J.-P., and C. Menkes, Propagation and reflection of long equatorial waves in the Pacific Ocean during the 1992–1993 El Niño, *J. Geophys. Res.*, *100*, 25,041–25,059, 1995.

Boulanger, J.-P., and C. Menkes, Long equatorial wave reflection in the Pacific Ocean from TOPEX/Poseidon data during the 1992–1998 period, *Clim. Dyn.*, *15*, 205–225, 1999.

Cane, M. A., and E. S. Sarachik, Forced baroclinic ocean motions, II, The linear equatorial bounded case, *J. Mar. Res.*, *35*, 395–432, 1977.

Chelton, D. B., R. A. de Szoeke, M. G. Schlax, K. El Naggar, and N. Siwertz, Geographical variability of the first baroclinic Rossby radius of deformation, *J. Phys. Oceanogr.*, *28*, 433–460, 1998.

Clarke, A. J., The reflection of equatorial waves from oceanic boundaries, *J. Phys. Oceanogr.*, *13*, 1193–1207, 1983.

Clarke, A. J., On the reflection and transmission of low-frequency energy at the irregular Pacific Ocean boundary, *J. Geophys. Res.*, *96*, 3307–3322, 1991.

Du Penhoat, Y., and M. Cane, Effect of low-latitude western boundary gaps on the reflection of equatorial motions, *J. Geophys. Res.*, *96*, 3307–3322, 1991.

Fu., L.-L., E. J. Christensen, C. Yamarone, M. lefebvre, Y. Menard, M. Dorrer, and P. Escudier, TOPEX/Poseidon mission overview, *J. Geophys. Res.*, *99*, 24,369–24,381, 1994.

Gill, A. E., *Atmosphere-Ocean Dynamics*, 662 pp., Academic, San Diego, Calif., 1982.

Godfrey, J., On ocean spin-down, I, A linear experiment, *J. Phys. Oceanogr.*, *5*, 399–409, 1975.

Hughes, R. L., The influence of thermocline slope on equatorial thermocline displacement, *Dyn. Atmos. Oceans*, *5*, 147–157, 1981.

Kessler, W. S., Observations of long Rossby waves in the northern tropical Pacific, *J. Geophys. Res.*, *95*, 5183–5217, 1990.

Kessler, W. S., and J. P. McCreary, The annual wind-driven Rossby wave in the sub-thermocline equatorial Pacific, *J. Phys. Oceanogr.*, *23*, 1192–1207, 1993.

Lukas, R., and E. Firing, The annual Rossby wave in the ventral equatorial Pacific ocean, *J. Phys. Oceanogr.*, *11*, 55–67, 1985.

Moore, D. W., Planetary-gravity waves in an equatorial ocean, Ph.D. thesis, 201 pp., Harvard Univ., Cambridge, Mass., 1968.

Moore, D. W., and S. G. Philander, Modeling the tropical oceanic circulation, in *The Sea*, vol. 6, edited by E. D. Goldberg, I. N. MaCave, J. J. O'Brien, and J. H. Steele, pp. 319–361, John Wiley, New York, 1977.

Pedlosky, J., The transparency of ocean barriers to Rossby waves: The Rossby slit problem, *J. Phys. Oceanogr.*, *31*, 336–352, 2001.

Picaut, J., F. Masia, and Y. duPenhoat, An advective-reflective conceptual model for the oscillatory nature of the ENSO, *Science*, *277*, 663–666, 1997.

Schopf, P. S., and M. J. Suarez, Vacillations in a coupled ocean-atmosphere model, *J. Atmos. Sci.*, *45*, 549–566, 1988.

Susanto, R. D., Q. Zheng, and X.-H. Yan, Complex singular value decomposition analysis of equatorial waves in the Pacific observed by TOPEX/Poseidon altimeter, *J. Atmos. Oceanic Technol.*, *15*, 764–774, 1998.

White, W. B., and C.-K. Tai, Reflection of interannual Rossby waves at the maritime western boundary of the tropical Pacific, *J, Geophys, Res,*, *97*, 14,305–14,322, 1992.

White, W. B., S. E. Pazan, and M. Inoue, Hindcast/forcast of ENSO events based upon the redistribution of observed and model heat content in the western tropical Pacific, *J. Phys. Oceanogr.*, *17*, 264–280, 1987.

White, W. B., N. Graham, and C.-K. Tai, Reflection of annual Rossby waves at the maritime western boundary of the tropical Pacific, *J. Geophys. Res.*, *95*, 3101–3116, 1990.

Wunsch, C., and A. E. Gill, Observations of equatorially trapped waves in Pacific sea level variations, *Deep Sea Res.*, *23*, 371–390, 1976.

Wunsch, C., and D. Stammer, The global frequency-wavenumber spectrum of oceanic variability estimated from TOPEX/Poseidon altimeter measurements, *J. Geophys. Res.*, *100*, 24,895–24,910, 1995.

L.-L. Fu, Jet Propulsion Laboratory, California Institute of Technology, Pasadena, CA 91109, USA.

X. Zang and C. Wunsch, Department of Earth, Atmospheric and Planetary Sciences, Massachusetts Institute of Technology, Cambridge, MA 02139, USA. (xiaoyun@pimms.mit.edu)